Macromolecules **2006,** *39,* 3901−3906

High-Dielectric-Constant Self-Assembled Nodular Structures in Polymer/Gold Nanoparticle Films

Valeriy V. Ginzburg,* Kyle Myers, Sarah Malowinski,† Robert Cieslinski, Michael Elwell, and Mark Bernius

The Dow Chemical Company, Core R&D, Midland, Michigan 48674

Received October 21, 2005; Revised Manuscript Received March 3, 2006

ABSTRACT: We utilize spin-casting and ultraviolet (UV) light-induced polymerization to make organic−inorganic nanocomposite thin films. The initial mixture consists of polycaprolactone (PCL) stabilized gold nanoparticles, reactive monomer alkoxytitanium triacrylate, and photoinitiator benzophenone, dissolved in *n*-butyl acetate (BuAc) solvent. Upon spin-casting and under UV light, solvent evaporates and triacrylate monomer undergoes polymerization, forming a hybrid film exhibiting complex morphologies on several length scales. In particular, we observe a controlled core−shell microdomain assembly of metal nanoparticles, compatibilizer, and metal-infused photo-cross-linkable acrylate polymer host. The composite film also exhibits high electrical capacitance due to the large effective dielectric constant of the metal nanoparticle-rich "nodules". We characterize the morphology of the film using both polarized light optical, transmission electron (TEM), and atomic force (AFM) microscopy and propose a theoretical model explaining the formation of macro- and microphase-separated structures. Our results demonstrate a route to engage molecular self-assembly in an organometallic hybrid composite which achieves unexpected and unusual material properties that could be used in the electronics industry.

Introduction

Self-assembly of nanoparticles and polymers into hybrid organic−inorganic structures is now a very promising avenue of creating materials with interesting and unexpected mechanical, optical, electronic, and other properties.[1−3] Unlike their more conventional counterparts, nanoparticles ($R \sim 2-20$ nm), especially when stabilized by appropriate ligands, can self-assemble together within a polymer matrix to form thermodynamically equilibrium—or at least metastable—structures. As shown both experimentally[1−5] and theoretically,[6,7] mixtures of nanoparticles and diblock copolymers result in the formation of microphase-separated structures in which particles typically segregate into one ("preferred") microdomain. Because of this microphase separation, particle-rich domains can have high electrical conductivity,[8] refractive index,[9] or mechanical strength, leading to the potential application of such materials for electronic, photonic, or biomedical purposes.

Our current study was prompted by another interesting potential application for polymer−inorganic nanocomposites—high dielectric constant (high-κ) materials. Such materials are of great interest to the electronics industry as potential gate dielectrics that would enable the operation of printed transistors using lower voltages.[10] Typical polymer materials have dielectric constant in the range $2 < \kappa < 5$, while ideal gate dielectrics should have $\kappa > 10$. One possible solution would be to create hybrid organic−inorganic films where polymeric ("organic") matrix would provide structural properties (strength and flexibility), while inorganic inclusions would have very high dielectric constant. Given appropriate morphological arrangements of two phases, the composite material would have sufficiently high dielectric constant ($\kappa > 10$ in the frequency range $1-10^6$ Hz). Recently, Rao and co-workers[11] prepared such composite using conductive microparticles of gold or silver (radius in the range $1-50$ μm) as the inorganic fillers; Popielarz et al.[12] obtained similar results using ceramic (barium titanate) particles. While these results are important and interesting, the use of micron-size fillers creates inherent limitation in terms of the minimum thickness of the dielectric gate film. Even when filler size is close to 1 μm, film thickness should be at least 10 μm or more. To make really thin (<5 μm) high-κ films, one needs to use conductive or high-κ ceramic nanoparticle fillers. Thus, issues of morphological self-assembly in multicomponent solvent/polymer/nanoparticle mixtures once again become critical.

Despite the widespread interest in nanoparticle−polymer composites, understanding of their behavior (both equilibrium and nonequilibrium) is still sketchy. In particular, much of theoretical work so far has been devoted to the equilibrium morphologies of the polymer/nanoparticle blend; little or no attention is paid to the role of solvents used to prepare films. In many instances, however, kinetic phenomena associated with film drying and large-scale phase separation can overshadow the nanoscale ordering. In this paper, we attempt to explain—qualitatively and semiquantitatively—the role of particles in morphology formation on both micro- and macroscale.

Results

Nanocomposite Film Preparation. In this study, we use the self-assembly of block copolymers and gold nanoparticles to prepare high-dielectric-constant ($\kappa > 10$) self-assembling nanocomposite films. Our system consists of polycaprolactone (PCL) ligand-stabilized gold nanoparticles, reactive alkoxytitanium triacrylate, and a photoresponsive initiator, benzophenone, dissolved in *n*-butyl acetate (BuAc) solvent. The solution is spin-cast onto an ozone-treated silicon substrate and exposed to 365 nm ultraviolet (UV) light. UV radiation induces photopolymerization of the acrylate double bond. Concomitantly, solvent evaporates, and the film solidifies, forming the final nanocomposite coating.

Several techniques are used to study the morphology of the film. We utilized polarized light optical microscopy to observe

---

* Corresponding author. E-mail: vvginzburg@dow.com.

† Present address: Instron Corp., 825 University Avenue, Norwood, MA 02062.

10.1021/ma052278n CCC: \$33.50

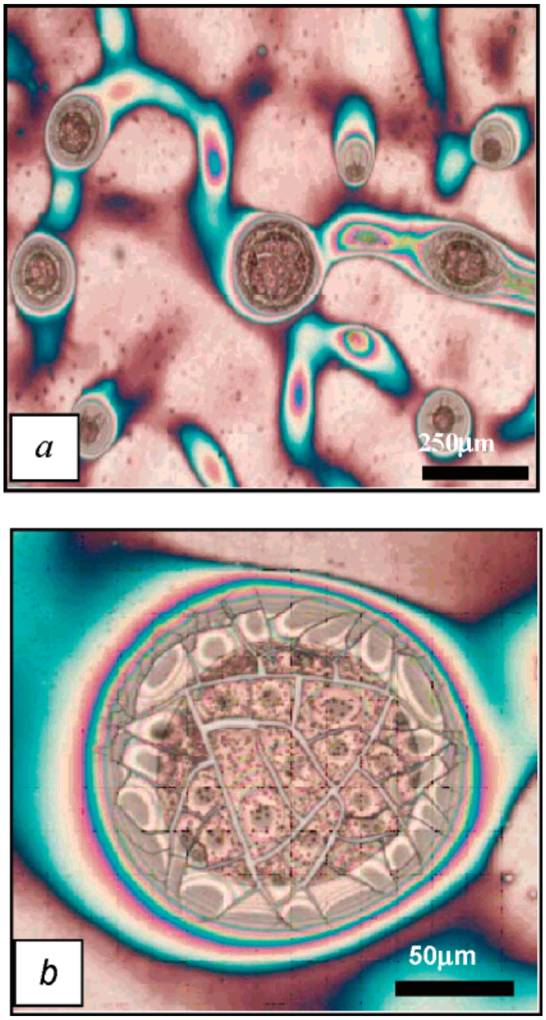

Figure 1. Cascading macrophase separation and nodule formation in polymer−nanoparticle film. (A) Large-scale polarized light optical micrograph showing phase-separated morphology of the dried film. (B) Magnified image of one nodule showing secondary and tertiary phase separation in its interior.

the features of the macrophase separation and atomic force microscopy [AFM] to investigate variations in film thickness. Subsequently, we performed transmission electron microscopy [TEM] measurements to study nanoscale dispersion of the Au nanoparticles.

Film Morphology: Macrophase Separation. Optical micrographs of the film produced with this technique are shown in Figure 1a,b. It can be seen clearly that the final material consists of numerous "core−shell"-type nodules of various sizes, distributed randomly in the main cross-linked polymer matrix. It can be also seen that there is partial dewetting of the film from the substrate. Close examination of parts a and b of Figure 1 shows that the nodules are the result of a complex, "cascading" phase separation process.

A simplified theoretical scheme of this process—based on a simple Flory−Huggins[13] treatment of the mixture—is given in Figure 2. We assumed that monomers were molecularly soluble in the BuAc solvent, and PCL-covered nanoparticles were fully dispersible in the same solvent; thus, at the beginning, the system could be considered homogeneous (one-phase). As matrix polymer built up its molecular weight, it becomes less and less soluble in the BuAc solvent, and one can observe the so-called polymerization-induced phase separation (PIPS). Looking at Figure 2a, one can see this effect in the change in the position of spinodal curves as a function of the polymer degree of polymerization N: as N goes up, the spinodal region moves toward lower values of the Flory−Huggins miscibility parameter χ. We estimate that Flory−Huggins parameter between butyl acetate solvent and PMMA polymer, χ(Pol−Solv) ~ 0.5−1. (It is somewhat difficult to evaluate it more precisely because of a large number of additives affecting the phase compositions.) In Figure 2b, we magnify this region and schematically chart the "phase trajectory" of the system as solvent evaporates and polymer molecular weight increases. Below, we describe the process in more detail.

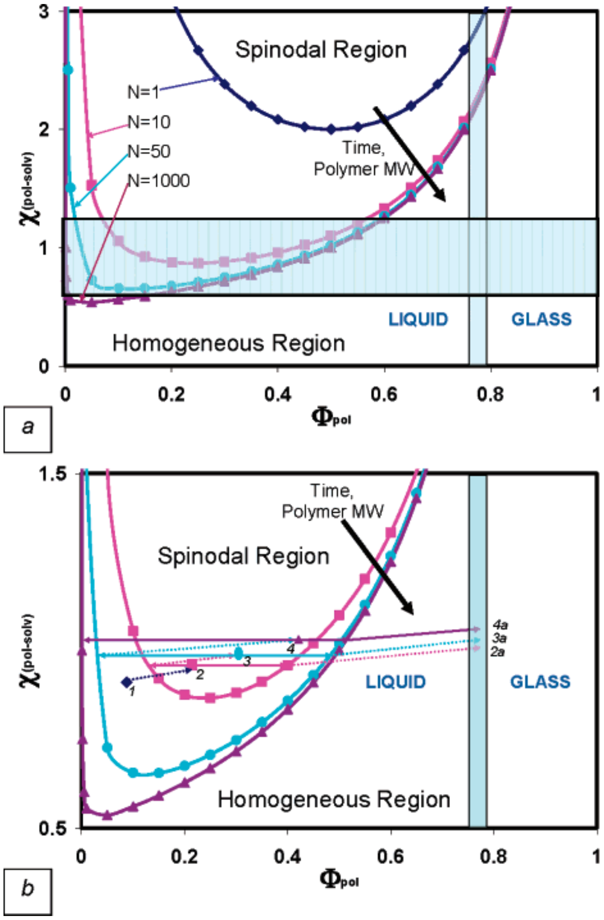

Figure 2. Qualitative Flory−Huggins phase diagram depicting proposed mechanism for the cascading phase separation during solvent evaporation and matrix curing: (A) general phase diagram; (B) blowup of the smaller-χ region and schematic representation of the system "trajectory" in phase space. See text for more details.

At the beginning (right after spin-coating, before solvent evaporation and polymer curing), the system is fairly homogeneous (point 1). As the polymerization proceeds and the solvent evaporates, the mixture moves into the spinodal region (point 2). In accordance with the standard spinodal decomposition (SD) scenario, long-wavelength density fluctuations begin to develop, separating polymer-rich and solvent-rich regions. Because of high viscosity of the polymer-rich regions (they are very close to vitrification point), there is very little structure development, and they remain relatively homogeneous. Subsequent evaporation of solvent leads to their complete vitrification (point 2a). Within solvent-rich regions, on the other hand, both polymers and solvent molecules are still fairly mobile. Further solvent evaporation within those regions shifts them again into the two-phase spinodal region (point 3)—once again causing separation of the system into solvent-rich and polymer-rich areas. Solvent-rich areas (droplets) can still undergo further morphology

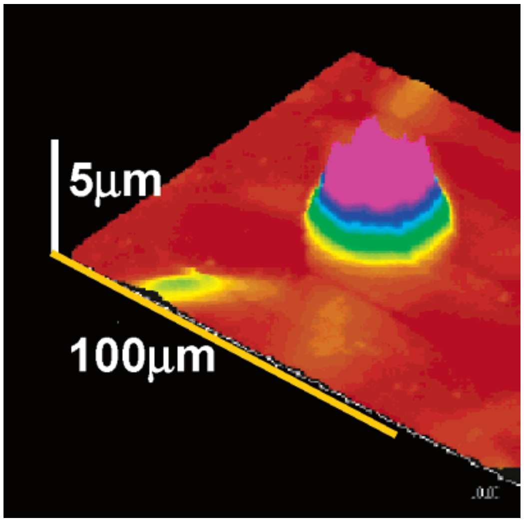

Figure 3. Atomic force microscope (AFM) image of a dried nodule.

development, while polymer-rich areas (strips between the droplets) vitrify very quickly (point 3a).[14] Inside the droplets, further evaporation of the solvent causes the system to become unstable yet again, resulting in the development of a new generation of spherical structures (point 4). This is, in our view, the reason for the formation of the nodules seen in Figure 1a,b. The process is similar to the cascading phase separation reported by Kyu and co-workers[15] for a polymer/liquid crystal binary mixture. However, in their system, phase separation is driven by polymerization only; in our case, both polymerization and solvent evaporation contribute to the cascading nature of the phase separation and nodule formation.[16] Important role is also played by the presence of the nanoparticles.[17]

Another striking feature of the films is the fact that the nodules have substantially larger height than the rest of the film. To better visualize the shape of a nodule, we utilized atomic force microscopy (AFM). As seen in Figure 3, the height of a nodule shown here is on the order of 4 μm, while the height of the film outside the nodules is only 50−100 nm. This buckling phenomenon is observed only in nanoparticle-containing systems; in control samples without nanoparticles, there was limited phase separation but no nodule formation. This result brings to memory a recent observation by Tsapis et al.[21] that the addition of colloidal particles can cause buckling in drying droplets. They associate the buckling with the onset of the liquid-to-solid transition in the shell of the drying droplet occurring when attractive capillary forces create a close-packed particle arrangement. A similar phenomenon can occur in the system described here—as the particles are localized due to the phase separation, the nodule walls stiffen and solidify. Another confirmation of this conjecture is the fact that after some time nodules exhibit shrinkage and cracking, indicating that their surfaces are solid and brittle. Obviously, more data are needed to better understand this complex phenomenon.

Polymer/Nanoparticle Self-Assembly: Experiment and Theory. Let us now consider polymer/particle interactions in more detail. At first, nanoparticles are randomly dispersed in the system. Subsequently, as the phase separation occurs, nanoparticles primarily remain in the solvent-rich areas. As polymerization and cure of the acrylate continues, particles become more and more incompatible with the polymer-rich phase and begin to "crowd" the nodules. Within the nodules, nanoparticles, PCL ligands, and PMMA matrix are self-assembling into complex nanoscale morphologies. The proof of this can be seen on the transmission electron micrographs (TEM) of a section of one of the nodules (Figure 4a,b). One could clearly see the formation of a nanostructure where most of the particles are concentrated in oblong nanodomains. Particles do not percolate but sometimes touch each other to form small clusters. It is clear that the volume fraction of particles in these nanodomains is larger than the average particle volume fraction in the sample as a whole. The light regions contain gold nanoparticles, polycaprolactone ligand, and polyacrylate polymer, while the dark regions contain primarily

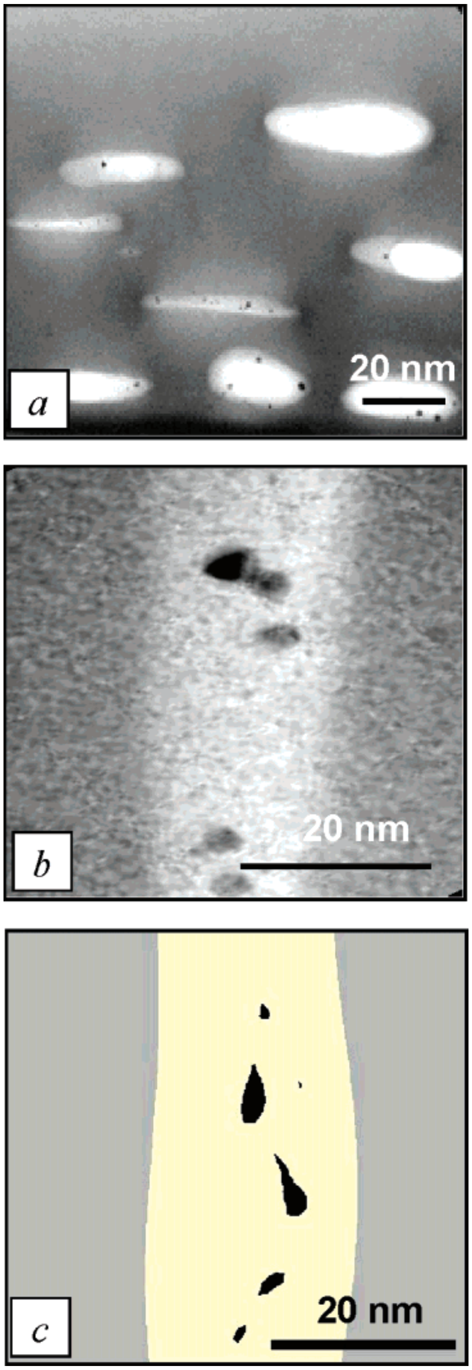

Figure 4. Structure formation and phase separation on a nanoscale. (A) TEM image of a section inside a nodule, indicating nanoscale segregation between two polymeric phases, with nanoparticles primarily confined into one (lighter) phase. (B) Magnified image of one "nanoparticle-rich" droplet and its vicinity. (C) Color map of the SCMFT simulation showing particle-rich (black), ligand-rich (yellow), and matrix polymer-rich (gray) regions. Simulation parameters: $\phi_P = 0.05$, $\phi_L = 0.40$, $\phi_M = 0.55$, $\chi_{PL} = 0.0$; $\chi_{PM} = 0.3$; $\chi_{ML} = 0.05$; $N_P = 200$; $N_L = 50$; $R_P = 5$ lattice units. Box size is 64 × 64.

polyacrylate polymer. The fact that particles are well-dispersed stems from the fact that (1) they are coated with long polycaprolactone oligomers to ensure strong steric repulsion and (2) polycaprolactone chains are well-miscible with solvent (BuAc) and acrylate monomer.

To better understand the morphology of the film on the nanoscale, we perform simulations of the system using the mean-field theory approach of Thompson, Ginzburg, Matsen, and Balazs (TGMB).[6,7] The TGMB model combines the real-space self-consistent-field theory of polymers (SCFT) with the Tarazona[18] formulation of a density functional formalism for spherical nanoparticles. In a particular case considered here, the free energy density of a nanoparticle/ligand/matrix ternary system can be written as

$$\frac{F}{k_B TV} = -n_M \ln\left(\frac{Q_M}{V\bar{\phi}_M}\right) - n_L \ln\left(\frac{Q_L}{V\bar{\phi}_L}\right) - n_P \ln\left(\frac{Q_P}{V\bar{\phi}_P}\right) + \frac{1}{V}\int d\mathbf{r}\, [\chi_{ML}\phi_M\phi_L + \chi_{MP}\phi_M\phi_P + \chi_{LP}\phi_L\phi_P - w_M\phi_M - w_L\phi_L - w_P\rho_P - \xi(1 - \phi_M - \phi_L - \phi_P)] \quad (1)$$

$$Q_P = V\bar{\phi}_P \exp\left\{-\frac{1}{Vn_P}\int d\mathbf{r}\, \rho_P[\ln(\rho_P) + \Psi_{CS}(\bar{\phi}\{\rho\})]\right\} \quad (2a)$$

$$\Psi_{CS}(x) = \frac{4x - 3x^2}{(1 - x)^2} \quad (2b)$$

$$\bar{\phi}\{\rho\}(\mathbf{r}) = \int_{|\mathbf{r} - \mathbf{r}'|<R_p} d\mathbf{r}'\, \rho(\mathbf{r}') \quad (2c)$$

$$Q_{M(L)} = \int d\mathbf{r}\, q_{M(L)}(\mathbf{r},1) \quad (3)$$

Here, indices M, L, and P denote matrix, ligand, and particle, respectively. Matrix polymer (PMMA), ligand (PCL), and particle number densities n_M, n_L, and n_P are related to the respective overall volume fractions $\bar{\phi}_M$, $\bar{\phi}_L$, and $\bar{\phi}_P$ in a standard way, $n_\alpha = \bar{\phi}_\alpha/v_\alpha$, α = M, L, P, and v_α is the volume of a matrix polymer, ligand polymer, or particle. Intermolecular interaction is described with the help of pairwise Flory–Huggins parameters, χ_{ML}, χ_{LP}, and χ_{MP}. The partition function for the particles, Q_P, is a functional of the particle center probability distribution, $\rho_P(\mathbf{r})$, and consists of the "ideal" and the "nonideal" Carnahan–Starling[19] term (first and second term in the square brackets in eq 2a). The explicit expressions used to calculate the nonideal term are given in eqs 2b and 2c and are based on the weighted density functional theory of Tarazona (see refs 6 and 18 for more details). The partition function for matrix (M) or ligand (L) homopolymer is given by eq 3, in which the propagator $q_{M(L)}(\mathbf{r},s)$ is the solution of a modified diffusion equation describing the conformations of a Gaussian homopolymer chain in external field $w_{M(L)}(\mathbf{r})$. The last term in square brackets is due to the incompressibility of the system, with ξ playing a role of pressure field. Minimization of the free energy (1) with respect to all fields and densities provides a set of self-consistency equations (see refs 6 and 7 for details). These equations are solved numerically using the real-space iterative algorithm of Fredrickson and Drolet.[20] Here we take the ligand degree of polymerization $N_L = 50$, the matrix polymer degree of polymerization $N_M = 200$, and the particle radius $R_P = 5$ lattice units ≈ 3 nm. Flory–Huggins parameters are chosen to reflect the strong preference of the particles to ligand polymer compared to the matrix polymer, $\chi_{ML} = 0.05$, $\chi_{LP} = 0.0$, and $\chi_{MP} = 0.3$. The mixture composition is chosen to closely reflect the real component balance once solvent evaporated completely: $\bar{\phi}_P = 0.05$, $\bar{\phi}_L = 0.40$, and $\bar{\phi}_M = 0.55$. Simulation is performed on a two-dimensional 64 × 64 square lattice, with 1 lattice unit = 3.5 Kuhn lengths = 2.1 nm. In Figure 4c we show the result of our calculation, with black areas corresponding to particles, yellow corresponding to ligand, and gray corresponding to the matrix polymer. Note that this is not equilibrium morphology, but rather a "kinetically trapped" state, both in simulation and in experiment. In simulations, kinetic trapping is due to finite size effects (boundary conditions prevent phase separation to continue on a scale beyond the box size); in experiments, it is due to the rapid cross-linking and vitrification of the polymer-rich regions. The fact that experiment and simulation are in a good qualitative agreement (cf. parts b and c of Figure 4) indicates that the phase separation and structure formation occur slowly enough for the system to be "near equilibrium" at all times. This, in turn, means that for such polymer/ligand/nanoparticle systems thermodynamics-based theories are good predictors of the particle dispersion and overall morphology and could be used for ligand, matrix, and nanoparticle selection and screening.

Dielectric Constant Measurements of the Films. Because of the difference in composition between the nodules and the rest of the film, one could expect that there would be also a large variation in physical properties. In our study, we concentrated on the measurement of the dielectric constant κ and electrical resistance R. We utilize the alternating current (ac) capacitance method to evaluate the dielectric properties of the nodular film made up of the two sizes of core–shell microdomains surrounded by a uniform polymer base. A highly conducting silicon wafer is used as a substrate and one electrode of capacitor geometry. The polymer matrix—once spun on and UV-cured—is then dried at 90 °C for 2 h in an oven to remove any solvents. The sample is then transferred to a physical vapor deposition (PVD) vacuum system where seven identical capacitor pads are deposited on the polymer film from a silver source. Thus, one substrate has 7-fold replication of the desired capacitor structure for purposes of experimental confidence in the data. The resulting capacitors are then tested in an ac precision LCR test station at 1.0 MHz frequency for the capacitance. Afterward, physical stylus profilometry is employed to determine the film thickness and the height/shape of the nodules. It is found that the complex cells are grouped into two categories. One group is comprised of smaller cells ~30 μm in diameter and 2.0 μm height. The second group consists of larger cells about 150 μm in diameter and 4.8 μm high. There is very little deviation from this size formation, and the size and distribution of these structures in the film are very uniform. Visually, their substructures are identical. Each capacitor pad for electrical testing contains between 97 and 102 large cells and between 91 and 126 small ones. This is seen over several wafers prepared on two different days from the stock solution.

To estimate the dielectric constant of the nodules, we adopt a parallel capacitor model. Specifically, we assume that our film consists of three effective parallel capacitors: (1) pure polymer film, with total area A_0, effective thickness d_0, and effective dielectric constant κ_0; (2) large (primary phase separation) nodules, with total area A_L, effective thickness d_L, and effective dielectric constant κ_L; and (3) small (secondary phase separation) nodules, with total area A_S, effective thickness d_S, and effective dielectric constant κ_S. Assuming that $\kappa_L = \kappa_S = \kappa_n$ (dielectric constant of a nodule—the unknown variable that needs to be determined from capacitance measurements), we obtain for the overall film capacitance

$$C_T = \epsilon_0\left[\kappa_0\frac{A_0}{d_0} + \kappa_n\left\{\frac{A_L}{d_L} + \frac{A_S}{d_S}\right\}\right] \qquad (4)$$

By separately measuring the capacitance, C_0, of a control film (no particles) of area $A_c = A = A_0 + A_S + A_L$ and the same thickness d_0, we determine the dielectric constant of the polymer, κ_0. The dielectric constant of the micelles, κ_n, is then given by

$$\kappa_n = \left[\frac{C_T - C_0(A_0/[A_0 + A_S + A_L])}{\epsilon_0}\right]\left[\frac{A_L}{d_L} + \frac{A_S}{d_S}\right]^{-1} \qquad (5)$$

Our measurements (performed at the ac frequency of 1 MHz) yielded $C_T = 10.31$ nF, $C_0 = 4.17$ nF, $A_0 = 0.3175$ cm^2, $A_L = 0.0177$ cm^2, $A_S = 0.0007$ cm^2, $d_L = 3.35$ μm, and $d_S = 1.40$ μm. From eq 5 we obtain $\kappa_n \approx 1260$. This is a very high value, typical for ceramic and semiconductor materials but not for organic-based systems.[22] However, electrical resistivity of the sample, although drops by a factor of 4 compared to the control film, still remains reasonably high, suggesting that the nodules do not conduct, and therefore, there is no bulk percolation of the metal nanoparticles. It is possible that the high value of the dielectric constant is the direct result of the cascading phase-separated morphology of the nodules, but we are not aware of any model that would describe dielectric properties of such systems. Development of such model remains a task for the future.

Discussion

We used spin-coating to prepare polymer−gold nanoparticle film. Because of the interplay of several competing factors (solvent evaporation, acrylate polymerization and cross-linking, particle diffusion), film is characterized by several interesting structural features not previously observed in polymeric thin films. Among the most interesting features is the presence of hierarchically structured nodules (Figures 1b and 3). These nodules (having height of ∼4 μm and diameter ∼20 μm after drying) are extremely inhomogeneous and possess several structural features on smaller (micron and submicron) length scales. We interpret these features as evidence of secondary and tertiary phase separation.

What is the origin of this cascading phase separation? In our view, the process is driven by competing effects of solvent evaporation and solvent−polymer phase separation (accelerated by the cross-linking and perhaps by nanoparticles acting as nucleating agents). Initial nodules correspond to the formation of solvent-rich droplets during the initial stage of the phase separation; they are also enriched with nanoparticles compared to the rest of the film. In the rest of the film, vitrification occurs rapidly as the solvent evaporates and polymer cross-links; within the nodules, there is still sufficient mobility due to the excess of the solvent. Thus, the process repeats itself within the nodules, with secondary nodules forming in solvent-enriched regions; these secondary nodules are also attracting the nanoparticles. The same process can take place on a smaller scale perhaps as tertiary phase separation and so on until the size of the domains becomes too small to be resolved by optical microscopy.

Why the cascading structure is preserved in the final film? In principle, one would imagine that the hierarchical structure could be a transient phenomenon, but ultimately the polymer composition within the film should equilibrate to a relatively uniform one. The only reason why the hierarchical structures exist even after the film dries completely is kinetic—the polymer-rich domains vitrify very quickly, and their subsequent coalescence is inhibited. One could speculate that if the rate of phase separation is much faster than the rate of vitrification, the film would ultimately have either homogeneous or a simple macrophase-separated structure (either translucent or opaque, but relatively flat and featureless film). If, on the other hand, the rate of vitrification is much higher than that of phase separation, the film would most certainly be uniform. Apparently, there is a small window of relative rates of phase separation and vitrification (or solvent evaporation) that can give rise to the formation of hierarchical nodules as observed in our experiments. A theoretical explanation of this phenomenon is still lacking.

Although we primarily discussed the solvent−polymer phase separation, it is clear that at each stage the polymer-rich phase is slightly different from the one at the previous stage. In principle, there can be additional polymer−polymer and polymer−particle phase separation. We believe that polymer−polymer and polymer−particle phase separation takes place primarily at the last stages of the process, when most of the solvent has evaporated. This results in a formation of various structures on the nanoscale that we investigated using TEM and computationally using SCMFT. In the PMMA/PCL/Au−NP mixture, PCL-rich domains with particles begin to separate from the PMMA matrix, as expected intuitively and as predicted by simulations. The growth and coalescence of these domains on a larger scale, however, is arrested by the ultimate vitrification of the film.

Because of the preferential segregation of the nanoparticles into the nodules and their subsequent segregation into secondary and tertiary “micelles”, the film acquires strongly nonhomogeneous distribution of its electrical properties. Regions with high particle concentration can be expected to have high dielectric polarizability and, therefore, high dielectric constant. This, indeed, was observed in our capacitance measurements.

Further studies are needed to elucidate the physics of the morphology formation in thin nanocomposite films under spin-coating. These studies should enable us to better understand the interplay between solvent evaporation rate, cross-linking rate, and nanoparticle size and concentration in determining the film structure. Such understanding, in turn, would be crucial in order to design more homogeneous films with high dielectric constant, $\kappa > 10$.

Conclusions

We prepared a self-assembled polymer/Au nanoparticle film using spin-cast deposition on a substrate and subsequent UV-cross-linking of the acrylate monomer. The resulting film exhibits a very interesting “nodular” morphology, with most of the Au nanoparticles localized in 3−4 μm high nodules. Optical microscopy indicates that inside these nodules further cascading phase separation continued, leading to the microstructure development at several length scales, from tens of nanometers to tens of microns. These conclusions are in agreement with our theoretical modeling based on the self-consistent mean-field theory of polymers and polymer/nanoparticle mixtures. We also show that the nodules exhibit very interesting physical properties, most notably very high dielectric constant combined with reasonably high electrical resistivity. It is expected that such materials hold significant promise for the development of future high-dielectric-constant gate polymers for printed electronics as well as for many other applications.[23,24]

Acknowledgment. We are thankful to The Dow Chemical Company for the support of this research. We are greatly indebted to anonymous reviewers for their helpful comments and suggestions.

CDV

References and Notes

(1) Alivisatos, A. P.; et al. *Adv. Mater.* **1998**, *10*, 1297 and references therein.

(2) Hamley, I. W. *Angew. Chem., Int. Ed.* **2003**, *42*, 1692 and references therein.

(3) Lopes, W.; Jaeger, H. M. *Nature (London)* **2001**, *414*, 735.

(4) Alivisatos, A. P. *Science* **1996**, *271*, 933.

(5) Bockstaller, M. R.; Lapetnikov, Y.; Margel, S.; Thomas, E. L. *J. Am. Chem. Soc.* **2003**, *125*, 5276.

(6) Thompson, R. B.; Ginzburg, V. V.; Matsen, M. W.; Balazs, A. C. *Science* **2001**, *292*, 2469; *Macromolecules* **2002**, *35*, 1060.

(7) Lee, J. Y.; Thompson, R. B.; Jasnow, D.; Balazs, A. C. *Phys. Rev. Lett.* **2003**, *91*, 136103. Lee, J. Y.; Thompson, R. B.; Balazs, A. C.; Hill, R. M. *Macromolecules* **2004**, *37*, 3536.

(8) Thurn-Albrecht, T.; et al. *Science* **2000**, *290*, 2126. Lin, Y.; et al. *Science* **2003**, *299*, 226.

(9) Edrington, A.; et al. *Adv. Mater.* **2001**, *13*, 421. Cheng, J. Y.; et al. *Adv. Mater.* **2001**, *13*, 1174. Bockstaller, M.; Kolb, R.; Thomas, E. L. *Adv. Mater.* **2001**, *13*, 1783.

(10) Wilk, G. D.; Wallace, A. M.; Anthony, J. M. *J. Appl. Phys.* **2001**, *89*, 5243.

(11) Rao, Y.; Wong, C. P.; Xu, J. High dielectric polymer composites and methods of preparation thereof. US Patent 6,864,306, 2005.

(12) Popielarz, R.; Chiang, C. K.; Nozaki, R.; Obrzut, J. *Macromolecules* **2001**, *34*, 5910.

(13) Flory, P. J. *J. Chem. Phys.* **1941**, *9*, 660. Huggins, M. *J. Chem. Phys.* **1941**, *9*, 440.

(14) In principle, there can be additional macrophase separation inside the polymer-rich regions (for example, between cross-linking acrylate matrix and PCL chains). This type of phase separation, however, would start at a later time than the solvent−polymer one and would be substantially slowed down by the vitrification of polymer-rich domains. Thus, PCL-rich and PMMA-rich domains would probably grow only within nanometer range (<100 nm), while the polymer−solvent phase separation would be primarily responsible for the structures developing on the micron length scale.

(15) Kim, J. Y.; Cho, C. H.; Palffy-Muhoray, P.; Kyu, T. *Phys. Rev. Lett.* **1993**, *71*, 2232.

(16) On the basis of thermodynamic considerations alone (Figure 2b), one could conjecture that cascading phase separation could occur even without cross-linking (driven purely by solvent evaporation). In that case, though, it is more likely that coalescence of polymer-rich domains would preempt their vitrification, and the multiscale pattern would not be observed. A comprehensive kinetic model combining the description of PIPS and solvent evaporation would be required to determine which conditions are necessary for the formation of multiscale nodules. To our knowledge, no such model exists at present time.

(17) In a similar cross-linking acrylate/PCL/BuAc system without gold particles, no nodules or multiscale self-similar structures were seen (films were either translucent or milky white, indicating some degree of macrophase separation). It is likely, therefore, that particles act as nuclei to start the phase separation and speed up its kinetics. Thus, in a system without particles, vitrification arrests the phase separation relatively early; in the presence of particles, vitrification stops the process only at its relatively late stage, with primary, secondary, and even tertiary phase separation well under way.

(18) Tarazona, P. *Mol. Phys.* **1984**, *52*, 81.

(19) Carnahan, N. F.; Starling, K. E. *J. Chem. Phys.* **1969**, *51*, 635.

(20) Drolet, F.; Fredrickson, G. H. *Phys. Rev. Lett.* **1999**, *83*, 4317; *Macromolecules* **2001**, *34*, 5317.

(21) Tsapis, N.; et al. *Phys. Rev. Lett.* **2005**, *94*, 018302.

(22) Our estimates of the dielectric constant of the nodule assume that dielectric properties inside the nodule remain constant or vary smoothly as a function of position. Further investigation is needed to confirm or disprove this assumption.

(23) Although the films with "nodular" structure provide relatively high capacitance and dielectric constant, they are not quite applicable for the use in electronics industry precisely because of their heterogeneity. However, we were also able to obtain high-dielectric-constant nanocomposites with more homogeneous structure.[24]

(24) Bernius, M.; Drumright, R.; Elwell, M. High Dielectric Constant Composites. US Patent Application 20040180988, 2004.

MA052278N